

Experimental studies of partial photodetachment cross sections in K^- below the $K(7^2P)$ thresholdA. O. Lindahl,^{1,*} J. Rohlén,¹ H. Hultgren,^{1,2} I. Yu. Kiyán,² D. J. Pegg,³ C. W. Walter,⁴ and D. Hanstorp^{1,†}¹*Department of Physics, University of Gothenburg, 41296 Gothenburg, Sweden*²*Albert-Ludwigs-Universität, D-79104 Freiburg, Germany*³*Department of Physics, University of Tennessee, Knoxville, Tennessee 37996, USA*⁴*Department of Physics and Astronomy, Denison University, Granville, Ohio 43023, USA*

(Received 5 December 2011; published 13 March 2012)

A collinear beams apparatus has been used to determine photodetachment cross sections for K^- in the photon energy range 4.250–4.360 eV. State-selective detection, utilizing a resonance ionization scheme, was applied to measure partial cross sections for those channels which leave the residual K atoms in the excited 7^2S , 5^2F , and 5^2G states. The energy region studied encompassed the openings of the aforementioned channels, as well as the channel that leaves the K atom in the 7^2P state. Two previously unobserved resonances were seen in all three partial cross sections between the $K(5^2G)$ and $K(7^2P)$ thresholds. It is shown that a more reliable determination of resonance parameters can be made if the same resonances are observed in several channels. In the region below the $K(5^2F)$ threshold, three previously observed resonances were investigated [Kiyán *et al.*, *Phys. Rev. Lett.* **84**, 5979 (2000)]. A greatly increased modulation of the signal was obtained by detecting in the $K(7^2S)$ channel instead of the $K(5^2S)$ channel used in the previous study. Furthermore, the shapes of the cross sections in the threshold regions are discussed. A detailed description of the apparatus and the experimental procedure employed is presented in the paper.

DOI: [10.1103/PhysRevA.85.033415](https://doi.org/10.1103/PhysRevA.85.033415)

PACS number(s): 32.80.Gc, 32.80.Zb, 32.80.Rm

I. INTRODUCTION

The structure and reaction dynamics of negative ions are of fundamental interest. Due to the nature of the binding of the outermost electron in negative ions, they are significantly different from atoms and positive ions. The interaction in atoms and positive ions can be described by a Coulomb potential when the electron is at large distances from the core. A consequence of this is the infinite series of Rydberg states. In negative ions, on the other hand, the asymptotic potential is described by a much shorter range induced dipole potential. If the extra electron is close to the parent atom, a full many-body treatment is needed to describe the interaction. The short-range potential is able to bind only a finite number of states. Atomic negative ions usually have only a single bound state. The binding energy is typically one order of magnitude smaller than that of the isoelectronic atom. The standard method to gain information about the structure of negative ions is through the photodetachment process, in which an electron is emitted due to the absorption of a photon. Valuable information regarding electron-electron correlation can be obtained by comparing photodetachment data with results from atomic many-body calculations.

The general lack of bound excited states in negative ions excludes the observation of bound-bound transitions in most ions. In the continuum above the detachment limit, however, there exists a rich spectrum of doubly excited states. Some of these states have configurations that can be excited with single-photon transitions from the ion ground state. These states can be viewed as an atom in an excited state to which an additional electron is attached. Doubly excited states are unstable and have lifetimes on the order of picoseconds. They

decay via autodetachment to a neutral atom and a free electron. The properties of such states are substantially influenced by the effects of electron-electron correlation. A great amount of theoretical and experimental effort has been devoted to the prototype negative ion, H^- [1–7]. Here, two electrons move in the pure Coulomb field of the nucleus; a case resembling the helium atom. The negative ions of the alkali metals can be considered to be quasi-two-electron systems in the frozen-core approximation. This is especially true for high-lying doubly excited states, where the effects of penetration and polarization of the core are smaller. Previous experimental work in the field includes studies of Li^- [8,9], Na^- [10], and K^- [11].

An interesting energy region is that just above the threshold for photodetachment. In this case the slow outgoing electron spends a significant time close to the core, and the interaction between the electron and the residual atom becomes very important. The photodetachment cross section just above threshold can be described by the Wigner law [12]. Wigner showed that it is the effective centrifugal potential that determines the shape of the threshold cross section, which is given by

$$\sigma \sim E_e^{\ell+1/2}, \quad (1)$$

where ℓ and E_e are the angular momentum and kinetic energy, respectively, of the outgoing electron. However, the energy range over which the dependency in Eq. (1) is valid is limited by the magnitude of other interactions such as the induced polarization interaction. O'Malley has developed a description that takes the polarizability of the residual atom into account [13], while the correction factor introduced by Farley describe the effect of the finite size of the initial-state wave function [14]. In an experiment reported by Sandström *et al.* [15] the threshold behaviors for photodetachment to final excited states with different, but large, positive polarizabilities were investigated. A modified effective range theory, developed

*anton.lindahl@physics.gu.se

†dag.hanstorp@physics.gu.se

by Watanabe and Greene [16], was successfully applied to the threshold data in this case. However, it is also possible for an excited atomic state to have a negative polarizability. This more unusual case was discussed in a recent publication [17] where the fundamentally different behaviors of the cross sections at the $K(5^2F)$ and $K(5^2G)$ thresholds were described. These two states have dipole polarizabilities of approximately the same large magnitude (10^6 a.u.), but with opposite sign [18]. A semiclassical model was developed to describe threshold cross sections in cases where the interaction in the final state is dominated by a negative polarizability of the residual atom. This model predicts a fundamentally different, exponential, energy dependence for the cross section given by the expression

$$\sigma \propto \exp[DE_e^{1/4}], \quad (2)$$

where the constant D depends on the polarizability as $D \propto |\alpha|^{1/4}$.

The present paper describes an investigation of the photodetachment of K^- . The experiment was performed using an upgraded collinear beams apparatus at the Göteborg University Negative Ion Laser Laboratory (GUNILLA). The apparatus and the experimental procedure employed are described in detail. The same facility was used in the study of threshold behaviors of the cross sections at the $K(5^2F)$ and $K(5^2G)$ thresholds [17] discussed above. In the present work, partial cross sections were measured for final-state channels leading to the formation of the residual K atom in the excited 7^2S , 5^2F , and 5^2G states. Two predicted resonances [18], which thus far have not been observed, were identified in the region between the $K(5^2G)$ and $K(7^2P)$ channel openings in all three partial cross sections. The advantage of investigating the same resonances in more than one detachment channel is illustrated in the paper. In the region between the $K(7^2S)$ and $K(5^2F)$ channel openings, three resonances were observed in the $K(7^2S)$ channel, in agreement with previous experimental [11] and theoretical [18] results. The measurements described in this paper were made possible by the use of an apparatus that combines high sensitivity and resolution with a high level of selectivity. This was achieved by a combination of a long collinear interaction region and a laser-based detection scheme.

II. EXPERIMENT

Figure 1 shows the optical excitation scheme used in the experiment. K^- ions were photodetached by UV photons generated by an optical parametric oscillator (OPO). The energy of the UV photons was substantially larger than the electron affinity of K, thus leaving the residual atoms in a distribution of final excited states. A state-selective detection scheme based on resonance ionization was used to measure the partial cross sections to specific excited states of the K atom. A second OPO generated infrared radiation and its photon energy was tuned to match the transition energy from a chosen excited state of K to a Rydberg state. The Rydberg atoms thus produced were field ionized in an electric field, enabling the resulting positive ions to be separated from the negative ions and the neutral atoms. The positive ions were detected

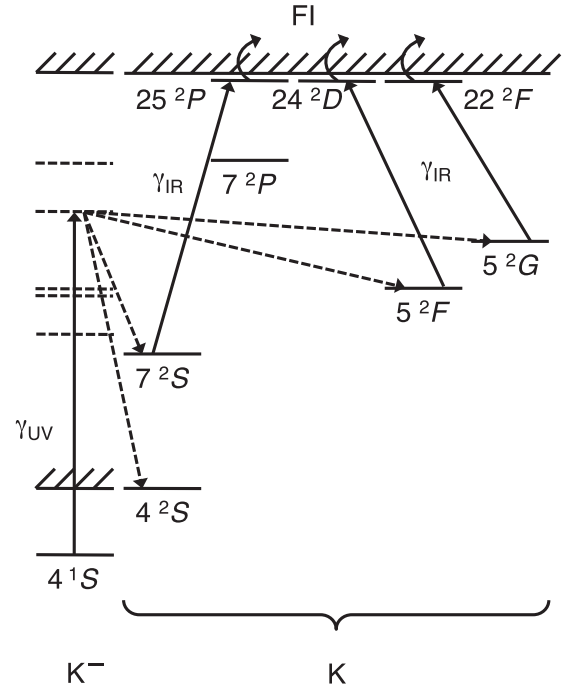
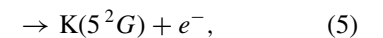
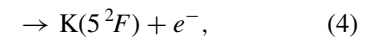
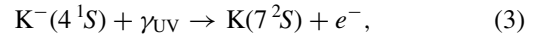


FIG. 1. Partial energy level diagram (not to scale) of the K^- and K systems. A K^- ion absorbs a UV photon (γ_{UV}) and is promoted to a doubly excited state (dashed energy levels), which decays via autodetachment (dashed arrows). State selectivity in the detection is achieved by resonant excitation using an IR photon (γ_{IR}) followed by field ionization (FI).

with a position sensitive detector. The three photodetachment channels studied in the present work are



which have threshold energies of 4.254 987(12), 4.296 210(14), and 4.297 522(12) eV respectively [19,20]. The main uncertainty in the threshold energies results from the uncertainty in the electron affinity of potassium, which is 0.501 459(12) eV [20]. The energy range studied includes the openings of the three aforementioned channels as well as that of the $K(7^2P)$ channel, which has a threshold energy of 4.353 636(14) eV.

Measurement of the partial cross sections to highly excited final states requires a method with high sensitivity and resolution and a high level of selectivity. A high sensitivity is needed since such cross sections are generally very small. The magnitude of the partial cross section for the $K(7^2S)$ channel, for example, is predicted to be only 0.008 Mb at 4.26 eV [18]. The sensitivity of the measurement was enhanced by a large interaction volume, defined by the collinear overlap of the superimposed laser and ion beams, and by an efficient detection of the residual atoms. Furthermore, the energy separation of adjacent states is small at high levels of excitation, necessitating high energy resolution and selectivity in the final-state detection. The present experiment relies, for example, on the correct identification of the $K(5^2F)$ and $K(5^2G)$ channels, whose thresholds are separated by as little

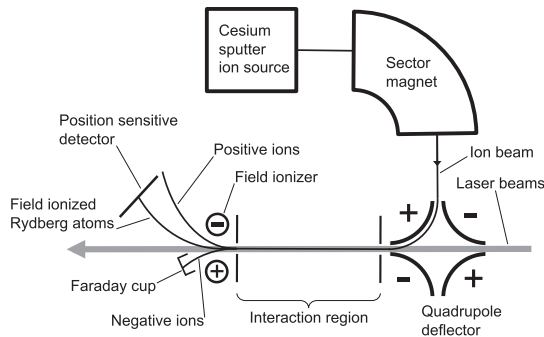


FIG. 2. Schematic of the collinear beams apparatus. Two laser beams and an ion beam are superimposed in a collinear copropagating geometry. The field ionizer separates the beam particles from the interaction region.

as 1.3 meV [19]. The state-selective detection of these atoms via resonance ionization was the basis for the high selectivity. The energy resolution was enhanced by the large reduction in kinematic broadening brought about by the collinear interaction of the ion and laser beams [21]. In the present measurement the energy resolution was determined primarily by the bandwidth of the laser used for photodetachment, which is approximately $25 \mu\text{eV}$.

The collinear laser and ion beams apparatus at GUNILLA is shown schematically in Fig. 2. Negative ions were produced in a cesium sputter ion source, from a sample of compressed K_2CO_3 powder, and were accelerated to 6 keV. A sector magnet was used for mass dispersion and a quadrupole deflector merged the ion beam with the laser beams. The beams were merged over a 61-cm-long interaction region defined by two apertures with a diameter of 3 mm. The ion current through the interaction region was typically on the order of 1 nA. The apparatus was recently upgraded to improve the mass resolution and the transmission through the interaction region, as described in detail by Diehl *et al.* [22]. The sector magnet was only single focusing; therefore, two single-focusing Einzel lenses were used in order to achieve a symmetric beam and improve the transmission through the system. The ion optics also included two Einzel lenses designed for symmetric focusing in two directions and a quadrupole triplet for beam shaping.

Two Nd:YAG-pumped OPOs were used in the experiment. They operated synchronously at a 10 Hz repetition rate and generated pulses of 6 ns duration and $25 \mu\text{eV}$ spectral bandwidth. The two OPOs have tuning ranges covering 0.65–5.6 eV and 0.25–0.92 eV, respectively. In the experiment, the photon energy of the UV radiation was tuned between 4.250 and 4.360 eV. The IR laser, on the other hand, was tuned to one of the resonant transitions $7^2S \rightarrow 25^2P$, $5^2F \rightarrow 24^2D$, and $5^2G \rightarrow 22^2F$, corresponding to photon energies of 562.050, 521.740, and 516.461 meV, respectively [19]. The UV and the IR beams were overlapped, copropagating with the ion beam. They were merged prior to the chamber using a mirror that reflected UV radiation and transmitted IR radiation. The pulse from the IR laser was triggered to arrive 50 ns after the UV laser pulse. The jitter in the delay time was on the order of a few nanoseconds. After the chamber the laser beams were separated by a Pellin-Broca prism. The pulse energies

of the two laser beams measured behind the interaction region were approximately 0.7 mJ for UV radiation and 0.2 mJ for IR radiation. With such energies, the nonresonant photodetachment transition driven by the UV radiation was far from saturation. The resonant transition driven by the IR radiation was saturated.

Optical parametric oscillators typically suffer from an inherent problem when used for high-resolution spectroscopy; namely, the center frequency jitters from pulse to pulse. The bandwidth of each pulse is small but the effective bandwidth, when averaged over several pulses, is larger. To overcome this problem, the wavelength of each UV pulse was measured using a commercially available wavelength meter. The absolute accuracy of the device was $2.5 \mu\text{eV}$. The wavelength meter was calibrated using a Doppler-free, saturated absorption measurement in Rb vapor. The UV pulse energy and the ion current were measured for each laser pulse and stored together with the measured wavelength and the output from the detector (described in detail below). A thorough description of the data acquisition system can be found in the earlier paper by Andersson *et al.* [23]. In the analysis of the data, which was done offline, all the data were binned according to the measured photon energy of the UV radiation.

The high velocity of the unidirectional ions moving collinearly with respect to the laser beam causes a Doppler shift. A correction for this shift was made by calculating the ion velocity from the known acceleration voltage in the ion source. The uncertainty of the ion beam kinetic energy gave an error in the corrected photon energy of less than $20 \mu\text{eV}$, which is on the order of the laser bandwidth. The calibration of the photon energy scale was confirmed by the observation of the known position of the sharp onset of the $\text{K}(5^2F)$ threshold.

State-selective detection of the K atoms in Rydberg states was achieved by using a combination of an electric field ionizer and a position sensitive detector. An inhomogeneous electric field was produced in the field ionizer, which consisted of two cylindrical electrodes placed 2 cm apart, as illustrated in Fig. 2. The electrodes were symmetrically biased with positive and negative voltages on the order of 4 kV. The field strength varied along the beam axis, having its maximum value between the two electrodes. Negative ions entering the field region were deflected into a Faraday cup. Rydberg atoms followed a straight path until the field strength was sufficient for field ionization to occur. Once ionized, the positive ions were deflected by the same field and finally detected with a position sensitive detector placed approximately 10 cm from the field ionizer. Atoms in different Rydberg states have different binding energies and were ionized at different positions along the path through the field ionizer. They therefore followed different trajectories and hit the position sensitive detector at different positions.

The position sensitive detector consists of a microchannel-plate (MCP) stack positioned in front of a pair of delay line anodes [24]. The active area of the detector has a diameter of 40 mm. Signals from the delay lines and the MCPs were amplified and converted to timing pulses by constant fraction discriminators. The timing pulses were digitized in a time-to-digital converter (TDC) with a 25 ps time resolution. The accumulated TDC data were used to calculate the position and time of arrival of positive ions at the detector. The velocity of

the 6 keV K^- ions was approximately $0.17 \text{ m}/\mu\text{s}$. This gives a time of flight from the interaction region to the detector of between 1 and $4.5 \mu\text{s}$.

A background of positive ions was caused by sequential two-electron detachment induced by the UV laser and by collisional double detachment of negative ions with the residual gas in the interaction chamber. A pressure of 10^{-8} to 10^{-9} mbar in the interaction chamber minimized the collisional events, leaving the photoinduced background as the dominant one. These background ions were immediately deflected by the electric field when they entered the field ionizer. Therefore, they followed a different path compared to that of the positive ions created by field ionization of Rydberg atoms, which constituted the signal in the experiment. Signal and background ions were thus spatially well separated at the detector. However, the multihit dead-time of the detector limited the maximum count rate for which individual hits could be unambiguously identified. This problem was minimized by adjusting the voltage of the field ionizer electrodes such that background ions were directed outside the active area of the detector. The trajectories of the ions through the field ionizer are illustrated in Fig. 2.

A known problem in experiments utilizing UV radiation and MCP-based detectors is that scattered light can potentially saturate the detectors. This problem was avoided by reducing the potential across the MCP stack during a time interval that covered the duration of the UV laser pulse. In the presence of the laser pulse, the front of the MCP stack was biased at $+800 \text{ V}$, while the back was at the operational $+2.2 \text{ kV}$, giving a voltage over the MCP stack of 1.4 kV . After the UV pulse, the front was set to ground potential, hence increasing the voltage across the MCP stack to the operational value of 2.2 kV . The switching time of the front voltage was approximately $0.5 \mu\text{s}$. Hence, the MCP stack was inactive when the photons hit and active at the time when the particles produced in the interaction region arrived at the detector.

Ultraviolet photons also produced secondary particles as a result of reflections on windows and walls in the vacuum chamber. These particles arrived at the detector over a time span of approximately $10 \mu\text{s}$, which overlapped with the arrival times of the positive ions that constituted the signal. In addition, fast ions produced secondary particles when striking electrodes and walls of the vacuum chamber. Background originating from these two sources was spatially spread out and was slowly varying over the active area of the detector. The value of this contribution could therefore be estimated and subtracted from the signal. Figure 3 shows a cut across the detector through the distribution of detected particles. For each photon-energy bin in the data analysis, the number of counts in the area of the detector containing the signal (marked black in the figure) was integrated. The background was determined as the mean count density around the signal region (hatched in the figure) and was subtracted accordingly. No further background subtraction was performed. The mean number of counts per laser shot was then normalized according to the average ion current and mean number of UV photons in the corresponding laser pulses. As can be seen in Fig. 3, the background was not completely flat. The shape of the background varied with experimental parameters and thus the subtraction worked better for some data sets than others.

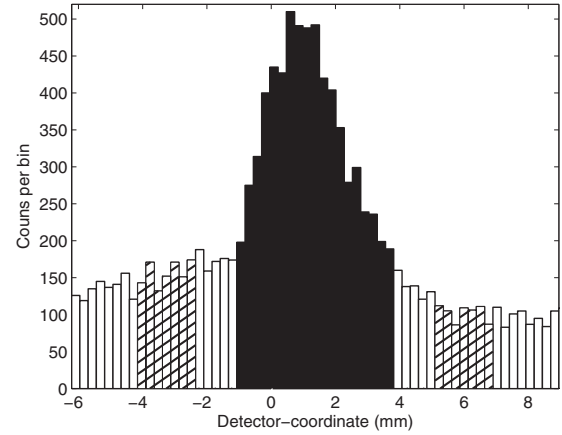


FIG. 3. Two-dimensional projection of the field-ionized Rydberg atoms in state 24^2D from measurement of the $K(5^2F)$ channel. The selected signal region is shown in black. The hatched regions are used to estimate the background in the signal region.

Mechanical and optical instabilities in the OPOs caused small pulse-to-pulse pointing instabilities in the laser beams. There might also have been a small drift of the UV beam direction as the wavelength was scanned. These effects were estimated to give uncertainties smaller than 10% within a measured cross section. Absolute measurements of cross sections are precluded, however, as a result of the unknown, and possibly changing, overlap of the ion and laser beams and the unknown efficiency of the detection system.

III. RESULTS

Figure 4(a) shows the partial photodetachment cross section for the $K(7^2S)$ channel from below the $K(7^2S)$ threshold to just above the $K(5^2F)$ channel opening. The region just below the $K(5^2F)$ threshold is shown in Fig. 4(b), where a second data set with higher point density is visible above 4.2955 eV . The signal is essentially zero below threshold and rises sharply at the threshold energy. The large modulations in the cross section above threshold are due to the presence of resonances in this region. The shape of such modulations can be described by the Fano parametrization using the energy E_r , the width Γ , and an asymmetry parameter q , [24] to model a resonance. An alternative, but equivalent, description of a resonance shape was given by Shore [26]. In the present work we extracted the resonance parameters by fitting the experimental data with an expression based on the Shore parametrization. The presence of resonant and nonresonant contributions was treated using the method presented by Liu and Starace [27]. The expression used in the fit includes a summation over multiple resonances and has the form

$$\sigma = (c + \hbar\omega d) \left(1 + \sum_i \frac{a_i \epsilon_i + b_i}{\epsilon_i^2 + 1} \right), \quad (6)$$

where i denotes the resonance index, $\hbar\omega$ is the photon energy, and $\epsilon_i = 2(\hbar\omega - E_{r,i})/\Gamma_i$ is a normalized energy parameter expressed in terms of the energy and the width of the i th resonance. The shape of a single resonance is described by the Shore parameters a_i and b_i . The nonresonant cross section

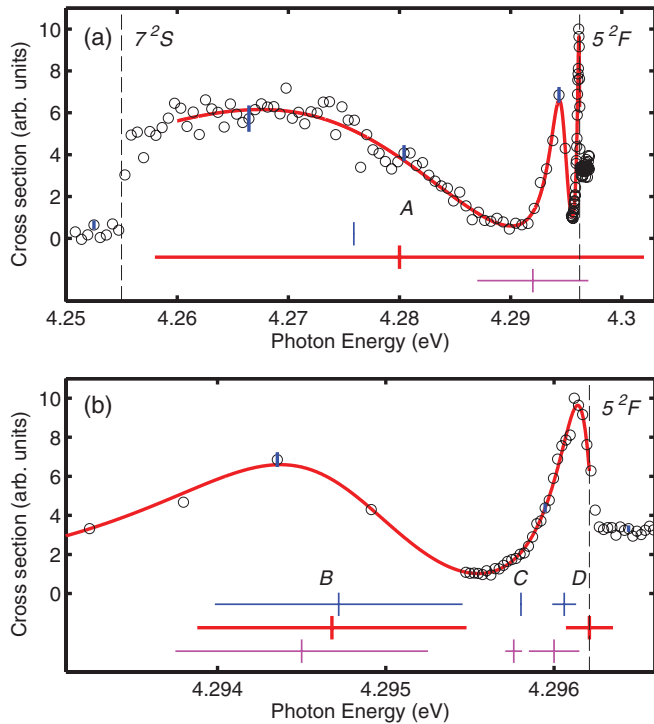


FIG. 4. (Color online) Partial cross section for the $K(7^2S)$ channel. Vertical dashed lines indicate threshold energies. Panel (a) shows the full energy region between the $K(7^2S)$ and the $K(5^2F)$ thresholds. Panel (b) shows a close-up of the region just below the $K(5^2F)$ threshold. Error bars (blue online) indicating the one sigma statistical uncertainty are shown for a few representative data points. The solid curve (red online) is a fit of Eq. (6) with three resonances. Resonance energies are shown as short vertical lines, while the horizontal lines indicate the widths. The lowest lines (magenta online) represent the previous experimental results by Kiyani *et al.* [11], the middle lines (red online) represent the present data, and the upper lines (blue online) are the theoretical values by Liu [18].

is represented by a linear function with coefficients c and d . The Fano shape parameter q_i was obtained from the best-fit values of a_i and b_i , according to the method of McDonald and Crowe [28]. Strictly speaking, the formula presented in Eq. (6) is valid only for isolated resonances [25,26]. In the present experiment some of the resonances are overlapping. Resonance A, for example, overlaps both resonances B and D. The width of A, however, is much larger than the widths of B and D. This means that the phase of the contribution from resonance A varies only a little over the other two resonances. Due to the small phase variation, the resonances can be treated individually with the parametrization in Eq. (6). For resonances B and D only the wings overlap; since the magnitude of this overlap is small the resonances can be treated as isolated to a good approximation.

The solid curves shown in Figs. 4(a) and 4(b) represent the best fit of Eq. (6) to the data. Contributions from three resonances are considered in this fit. The energies and widths that were extracted for resonances A, B, and D are presented in Table I and are marked in Fig. 4. Resonance C was not observed in the present experiment.

TABLE I. Resonance parameters extracted in the present experiment compared with previous results.

Label	Channel/source	E_r (eV)	Γ (meV)	q
A	$K(7^2S)$	4.28(2)	44(20)	-1.4
	$K(5^2S)^a$	4.292(2)	10 (2)	
	Calculation ^b	4.275 90		
B	$K(7^2S)$	4.294 68(9)	1.6 (3)	-2.8
	$K(5^2S)^a$	4.2945 (1)	1.5 (2)	
	Calculation ^b	4.294 72	1.472 2	
C	$K(7^2S)^c$			
	$K(5^2S)^a$	4.295 76(4)	0.10 (8)	
	Calculation ^b	4.295 803 1	0.002	
D	$K(7^2S)$	4.296 21(5)	0.28 (5)	-2.1
	$K(5^2S)^a$	4.2960(2)	0.30 (3)	
	Calculation ^b	4.296 06		
E	$K(7^2S)$	4.321(5)	19 (6)	0.5
	$K(5^2F)$	4.327(7)	26 (9)	
	$K(5^2G)$	4.325(4)	25 (8)	
	Mean ^d	4.324(3)	22 (5)	
	Calculation ^b	4.32339	27.718 3	
	$K(7^2S)^e$	4.320(3)	25 (9)	
	$K(7^2G)^e$	4.319(4)	27 (4)	
Mean ^e	4.320(3)	27 (4)		
F	$K(7^2S)$	4.353 2(6)	2.2 (5)	0.23
	$K(7^2F)$	4.353 2(5)	2.2 (4)	
	$K(7^2G)$	4.353 00(13)	1.66 (12)	
	Mean ^d	4.353 02(13)	1.72 (12)	
	Calculation ^b	4.353 50		

^aExperimental work performed by Kiyani *et al.* [11].

^bCalculation performed by Liu [18].

^cResonance not observed in present work.

^dWeighted mean of the parameters from the three channels in the present measurement.

^eParameters determined with a slightly smaller data set in Ref. [17].

Cross sections for the $K(7^2S)$, $K(5^2F)$, and $K(5^2G)$ photodetachment channels in the energy region 4.29–4.36 eV are shown in Fig. 5. This region encompasses the thresholds for the $K(5^2F)$, $K(5^2G)$, and $K(7^2P)$ channel openings. Two resonances are observed in all three partial cross sections. A relatively broad resonance appears at approximately 4.324 eV and a much narrower one is seen at 4.353 eV, just below the $K(7^2P)$ channel opening. Data sets with higher point density were used to resolve the structures around the narrow resonance. The threshold region for photodetachment to the $K(5^2F)$ channel [see Fig. 5(c)] looks much like a step function. In the $K(5^2G)$ channel [see Fig. 5(d)], in contrast, the photodetachment cross section is slowly increasing with energy above threshold. The signal below threshold in Fig. 5(c) is nonzero. This finite-valued baseline indicates that the background subtraction described in Sec. II is not completely successful in the $K(5^2F)$ channel. In comparison, the baselines in Figs. 4(a) and 5(d) align better with the zero line.

The data of the $K(7^2S)$ and $K(5^2F)$ channels were fit using Eq. (6) involving two resonance contributions. In the $K(5^2G)$ channel, the slowly varying cross section in the threshold region extends over the whole region up to the

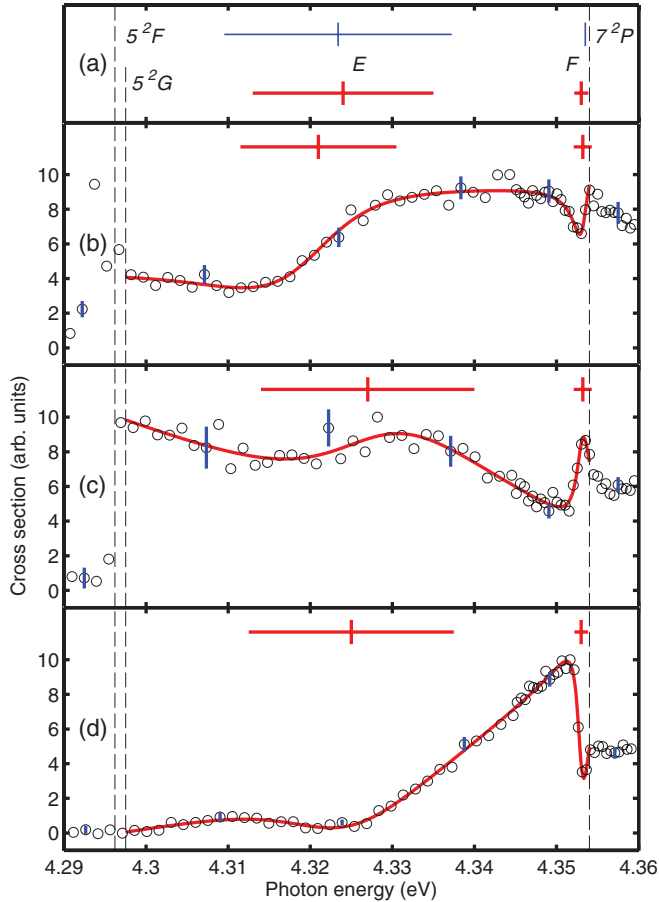


FIG. 5. (Color online) Partial photodetachment cross sections for the $K(7^2S)$, $K(5^2F)$, and $K(5^2G)$ channels, shown in panels (b), (c), and (d), respectively. Error bars (blue online) indicating the one sigma statistical uncertainty are shown for a few representative data points. Representative fits to the data are shown as solid curves (red online). Energies and widths of the resonances extracted from the three fits are indicated in the corresponding panels. Panel (a) shows the weighted mean of the resonance parameters (lower line, red online) as well as the values by Liu (upper line, blue online). Threshold energies are indicated by vertical dashed lines.

$K(7^2P)$ threshold. In this case, we replaced the linear part in Eq. (6), which represents the nonresonant cross section, with the threshold law from Eq. (2), yielding an expression

$$\sigma = \sigma_0 \exp[D(\hbar\omega - E_{5^2G})^{1/4}] \left(1 + \sum_i \frac{a_i \epsilon_i + b_i}{\epsilon_i^2 + 1} \right), \quad (7)$$

where σ_0 is a normalization parameter and E_{5^2G} is the threshold energy for the $K(5^2G)$ channel. The values for the resonance energies and widths extracted from these fits are also given in Table I. Resonance E has previously been investigated in the $K(7^2S)$ and $K(5^2G)$ channels [17]; these parameters are also presented in Table I. The values of the resonance parameters differ slightly between the previous and present study. Given the quoted uncertainties, however, the values are in agreement. The differences in the resonance parameters are due to differences in the fitting procedure, where, for example, resonance F is included in the fits in the present study. Moreover, the data in the present study were extended with the

detailed data sets above 4.345 eV in Fig. 5, compared to [17]. For all resonance energies presented in Table I, the 20 μeV uncertainty in the energy scale due to the Doppler shift was added in quadrature to the one-sigma uncertainty from the fit.

IV. DISCUSSION

The energy region between the $K(7^2S)$ and $K(5^2F)$ channel openings, as shown in Fig. 4, was previously investigated, both experimentally by Kiyani *et al.* [11] and theoretically by Liu [18]. Table I is a compilation of the energies and widths of the resonances determined in the present experiment and in previous studies. The cross section to the $K(7^2S)$ channel below the $K(5^2F)$ channel opening shows both similarities and differences with the previous two cross-section determinations. First we observe that the relative magnitude of the modulations differ although the general shape of the cross sections are similar. In the present experiment we observe a 90% modulation in the $K(7^2S)$ channel, whereas the $K(5^2S)$ channel investigated by Kiyani *et al.* exhibited a modulation of 25%. The larger modulation indicates that the reaction pathways via the doubly excited states are relatively more important in the $K(7^2S)$ channel than in the $K(5^2S)$ channel. This is an advantage if the increased relative modulation does not come at the cost of reduced overall signal level. A number of absolute partial cross sections for photodetachment of K^- have been calculated in [18]. These show a general trend that modulations due to resonances decrease slower than the level of the nonresonant cross sections for higher-lying final-state channels. Second, a very narrow resonance, labeled C in Table I and Fig. 4, was observed by both Kiyani *et al.* and Liu, but it is not visible in the present data. Apparently, the branching ratio into the $K(7^2S)$ channel was insufficient to produce a significant modulation in the present experiment. Third, the width of resonance A is more than four times greater than the width determined by Kiyani *et al.* As a consequence, the uncertainty in the resonance energy is also larger in the current experiment. This increased uncertainty is not caused by a lower statistical quality of the data, but is rather a consequence of the broader structure that is observed in the $K(7^2S)$ channel. It is obvious from the previous calculation [18] and experiment [11] and the present data that it is difficult to make a conclusive determination of the resonance parameters for resonance A. An experimental investigation of additional photodetachment channels would be needed in order to make a definite assignment of the energy and width of the associated doubly excited state.

There are two resonances present in all the three channels in the region between $K(5^2F)$ and $K(7^2P)$ thresholds (see Fig. 5). It is interesting that the general shapes of the cross-section curves in the three channels are very different, although the observed resonances are due to the same two doubly excited states. The energies and widths of the resonances should be the same in all three channels. Variations in shape are caused by different phase shifts in the interference in the different channels, which is described by the line shape parameters a_i and b_i (or q_i). The resonance positions are not obvious from inspection of the individual partial cross sections. Nevertheless, the fittings in each of the three channels produced very similar resonance parameters. The measured

parameters were also in good agreement with the energies and widths calculated by Liu [18]. These results clearly show the advantage of detecting the same resonance in more than one channel. This is particularly important in cases where resonances partially overlap each other.

V. CONCLUSIONS

We have developed an apparatus which enables the study of partial photodetachment cross sections to highly excited states of the residual atom, even when the cross sections are very small. The apparatus was used in the study of the $K(7^2S)$, $K(5^2F)$, and $K(5^2G)$ final-state detachment channels in the potassium negative ion. We have shown that it is an advantage to observe a resonance structure in more than one channel, as was illustrated for the resonances below the $K(7^2P)$ threshold. The experimental technique presented, where an IR laser is used for the resonance ionization, enables the detection of highly excited final states. This gives the possibility to select the most favorable of an increased number of channels. The best possible signal level and modulation of the cross section as well as noise and background levels can thus be achieved. This, in turn, leads to more reliable determinations

of resonance parameters. The ability to detect residual atoms in highly excited states has another advantage: It allows one to study the effect of high dipole polarizability on threshold behavior.

In the present experiment, parameters have been determined for two previously unobserved resonances between the $K(5^2G)$ and $K(7^2P)$ thresholds. The results are in good agreement with the previously calculated values by Liu [18]. This study, together with a recent paper [17], constitute the first step in an intended series of measurements with the aim of investigating photodetachment at an increasing degree of excitation. Our long-term goal is to access channels where the residual atom states are approaching the double detachment limit.

ACKNOWLEDGMENTS

Financial support from the Swedish Research Council is gratefully acknowledged. C.W.W. received support from the Wenner-Gren Foundation, the Andrew W. Mellon Foundation, and NSF Grants No. 757976 and No. 1068308. H.H. and I. Yu. K. acknowledge the support of the Deutsche Forschungsgemeinschaft, Grant No. KI 865/3-1.

-
- [1] W. Klopper, R. A. Bachorz, D. P. Tew, and C. Hättig, *Phys. Rev. A* **81**, 022503 (2010).
 - [2] K. R. Lykke, K. K. Murray, and W. C. Lineberger, *Phys. Rev. A* **43**, 6104 (1991).
 - [3] S. I. Themelis, *J. Chem. Phys.* **132**, 154111 (2010).
 - [4] E. Lindroth and J. L. Sanz-Vicario, *Radiat. Phys. Chem.* **70**, 387 (2004).
 - [5] P. Balling, H. H. Andersen, C. A. Brodie, U. V. Pedersen, V. V. Petrunin, M. K. Raarup, P. Steiner, and T. Andersen, *Phys. Rev. A* **61**, 022702 (2000).
 - [6] H. R. Sadeghpour and C. H. Greene, *Phys. Rev. Lett.* **65**, 313 (1990).
 - [7] P. G. Harris, H. C. Bryant, A. H. Mohagheghi, R. A. Reeder, H. Sharifian, C. Y. Tang, H. Tootoonchi, J. B. Donahue, C. R. Quick, D. C. Rislove, W. W. Smith, and J. E. Stewart, *Phys. Rev. Lett.* **65**, 309 (1990).
 - [8] U. Ljungblad, D. Hanstorp, U. Berzinsh, and D. J. Pegg, *Phys. Rev. Lett.* **77**, 3751 (1996).
 - [9] G. Haeflner, I. Yu. Kiyani, U. Berzinsh, D. Hanstorp, N. Brandefelt, E. Lindroth, and D. J. Pegg, *Phys. Rev. A* **63**, 053409 (2001).
 - [10] G. Haeflner, I. Yu. Kiyani, D. Hanstorp, B. J. Davies, and D. J. Pegg, *Phys. Rev. A* **59**, 3655 (1999).
 - [11] I. Yu. Kiyani, U. Berzinsh, J. Sandström, D. Hanstorp, and D. J. Pegg, *Phys. Rev. Lett.* **84**, 5979 (2000).
 - [12] E. P. Wigner, *Phys. Rev.* **73**, 1002 (1948).
 - [13] T. F. O'Malley, *Phys. Rev.* **137**, A1668 (1965).
 - [14] J. W. Farley, *Phys. Rev. A* **40**, 6286 (1989).
 - [15] J. Sandström, G. Haeflner, I. Yu. Kiyani, U. Berzinsh, D. Hanstorp, D. J. Pegg, J. C. Hunnell, and S. J. Ward, *Phys. Rev. A* **70**, 052707 (2004).
 - [16] S. Watanabe and C. H. Greene, *Phys. Rev. A* **22**, 158 (1980).
 - [17] A. O. Lindahl, J. Rohlén, H. Hultgren, I. Yu. Kiyani, D. J. Pegg, C. W. Walter, and D. Hanstorp, *Phys. Rev. Lett.* **108**, 033004 (2012).
 - [18] C.-N. Liu, *Phys. Rev. A* **64**, 052715 (2001).
 - [19] J. E. Sansonetti, *J. Phys. Chem. Ref. Data* **37**, 7 (2008).
 - [20] K. T. Andersson, J. Sandström, I. Yu. Kiyani, D. Hanstorp, and D. J. Pegg, *Phys. Rev. A* **62**, 022503 (2000).
 - [21] S. Kaufman, *Opt. Commun.* **17**, 309 (1976).
 - [22] C. Diehl, K. Wendt, A. O. Lindahl, P. Andersson, and D. Hanstorp, *Rev. Sci. Instrum.* **82**, 053302 (2011).
 - [23] P. Andersson, A. O. Lindahl, C. Alfredsson, L. Rogström, C. Diehl, D. J. Pegg, and D. Hanstorp, *J. Phys. B* **40**, 4097 (2007).
 - [24] Commercially available from RoentDek Handels GmbH.
 - [25] U. Fano, *Phys. Rev.* **124**, 1866 (1961).
 - [26] B. W. Shore, *Phys. Rev.* **171**, 43 (1968).
 - [27] C.-N. Liu and A. F. Starace, *Phys. Rev. A* **60**, 4647 (1999).
 - [28] D. G. McDonald and A. Crowe, *J. Phys. B* **26**, 2887 (1993).